RESEARCH ARTICLE | AUGUST 07 2023

Origin of medium-range atomic correlation in simple liquids: Density wave theory

Takeshi Egami ; Chae Woo Ryu

AIP Advances 13, 085308 (2023)
https://doi.org/10.1063/5.0159044

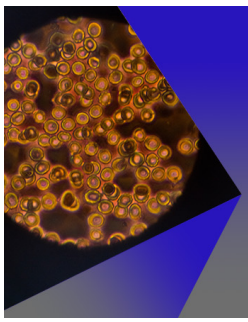

Origin of medium-range atomic correlation in simple liquids: Density wave theory

Cite as: AIP Advances 13, 085308 (2023); doi: 10.1063/5.0159044
Submitted: 19 May 2023 • Accepted: 15 July 2023 •
Published Online: 7 August 2023

Takeshi Egami[1,2,3,a] and Chae Woo Ryu[1,4]

AFFILIATIONS

[1] Shull-Wollan Center, Department of Materials Science and Engineering, University of Tennessee, Knoxville, Tennessee 37996, USA
[2] Department of Physics and Astronomy, University of Tennessee, Knoxville, Tennessee 37996, USA
[3] Materials Sciences and Technology Division, Oak Ridge National Laboratory, Oak Ridge, Tennessee 37831, USA
[4] Department of Materials Science and Engineering, Hongik University, Seoul 04066, South Korea

[a] Author to whom correspondence should be addressed: egami@utk.edu

ABSTRACT

The atomic pair-distribution function of simple liquid and glass shows exponentially decaying oscillations beyond the first peak, representing the medium-range order (MRO). The structural coherence length that characterizes the exponential decay increases with decreasing temperature and freezes at the glass transition. Conventionally, the structure of liquid and glass is elucidated by focusing on a center atom and its neighboring atom shell characterized by the short-range order (SRO) and describing the global structure in terms of overlapping local clusters of atoms as building units. However, this local *bottom-up* approach fails to explain the strong drive to form the MRO, which is different in nature from the SRO. We propose to add an alternative *top-down* approach based upon the density wave theory. In this approach, one starts with a high-density gas state and seeks to minimize the global potential energy in reciprocal space through density waves using the pseudopotential. The local bottom-up and global top-down driving forces are not mutually compatible, and the competition and compromise between them result in a final structure with the MRO. This even-handed approach provides a more intuitive explanation of the structure of simple liquid and glass.

I. INTRODUCTION

Liquid is a more condensed matter with density than solid. In liquid, atoms are bound together by attractive interatomic potential, and their movements are highly correlated. Its structure is not totally random, characterized by local order. How to determine and understand such local order in the atomic arrangement and how to relate it to properties, including the glass transition, are open and challenging questions.[1–5] The atomic structure of liquid and glass is usually described by the pair-distribution function (PDF), $g(r)$, which depicts the distribution of distances between two atoms,

$$g(r) = \frac{1}{4\pi N\rho_0 r^2}\sum_{i,j}\langle\delta(r-|\boldsymbol{r_i}-\boldsymbol{r_j}|)\rangle, \quad (1)$$

where $\boldsymbol{r_i}$ is the atomic position of the i-th atom, N is the number of atoms in the system, ρ_0 is the average number density of atoms, and $\langle\cdots\rangle$ denotes the thermal and ensemble average.[1,3,6] Nominally, the PDF describes only the two-body correlations, whereas properties of liquid and glass often depend on correlations of higher orders.[7–9] Nevertheless, the PDF is most widely used in describing the structure because it can be determined with high accuracy by x-rays or neutron diffraction measurement through the Fourier-transformation of the structure function, $S(Q)$, where Q is the momentum transfer of scattering.[1,3,6]

The PDF shows many peaks indicating shell-like structures around each atom. The first peak describes the short-range order (SRO) in the nearest neighbor shell, whereas the peaks beyond the first peak depict the medium-range order (MRO). A common approach to explain the glass structure is to consider how the nearest neighbor atoms of a central atom are configured and then try to figure out how the local structures are stacked up to form the MRO beyond the nearest neighbors.[1–3,10–13] This approach is successful in describing certain features of the second PDF peak in

terms of the topological MRO as combinations of local structural motifs.[14–16]

However, the SRO and the MRO beyond the second peak show various distinct behaviors, which cannot be readily explained by the bottom-up approach. For instance, in metallic liquids, the position of the first PDF peak, r_1, and that of the second peak, r_2, *decrease* with increasing temperature, whereas those of the higher order peaks increase following thermal expansion.[17,18] When supercooled liquid becomes glass through the glass transition at T_g, the MRO freezes whereas the SRO does not.[19] These distinct behaviors reflect the fundamental difference between the SRO and the MRO: they represent different kinds of correlations. The first peak of the PDF, which represents the SRO, describes the distribution of distances from the central atom to the nearest neighbors. The number of atoms involved, the coordination number, N_C, is 12–14 for simple liquids with a dense-random-packed (DRP) structure, such as metallic liquids,[2,3,20] and is less for covalent liquids. However, at longer distances, a PDF peak represents a much larger number of interatomic distances. The width of the higher-order peaks in the PDF is of the order of 1 Å, much wider than the typical phonon amplitudes, which are of the order of 0.1 Å. Therefore, the peaks in the PDF beyond the second neighbors do not represent individual interatomic distances, but instead they describe more coarse-grained local density fluctuations.[21] In other words, the first peak describes the correlations between two atoms, but the MRO describes the correlations between atom and density fluctuations. The second peak is mixed in nature.

For this reason, even though the PDF is a two-body correlation function, some features of the MRO reflect those of higher-order correlations; the derivative of the PDF depends on three-body correlation among two atoms separated by r and the third atom at $r + dr$. A piece of evidence that the MRO represents a different kind of correlation from the SRO is the observation that correlations between atoms in the MRO range decay with time more slowly than those among the nearest neighbors.[22] The decay of correlation with time is best expressed by the Van Hove function (VHF), $G(r, t)$,[23]

$$G(r,t) = \frac{1}{4\pi N\rho_0 r^2}\sum_{i,j}\langle\delta(r - |\boldsymbol{r_i}(0) - \boldsymbol{r_j}(t)|)\rangle, \tag{2}$$

where $\boldsymbol{r_i}(t)$ is the position of the i-th atom at time t. From the decay of the VHF peak height with time, the decorrelation time, τ, can be determined. For high temperature liquids, it was found that τ beyond the first peak depends both on distance and dimension by

$$\tau(r) = \tau_0 + \tau_r\left(\frac{r}{a}\right)^{\chi}, \quad \chi = \frac{d-1}{2}, \tag{3}$$

where a is the nearest neighbor distance defined by the first maximum in the PDF and d is the dimensionality.[22] This dependence on distance and dimension originates from the fact that $\tau(r)$ beyond the first neighbors describes the statistical timescale of local density fluctuations rather than the timescale of atom–atom correlations. The number of atoms in the shell between r and $r + dr$, $N_r dr$, increases with r as $N_r \propto r^{d-1}$, so the number fluctuation is proportional to $\sqrt{N_r}$ and thus to $r^{(d-1)/2}$, as shown in Eq. (3), resulting in the linear increase in $\tau(r)$ with r for three dimensions.

In this work, we discuss the origin of the MRO by proposing a top-down approach, by starting with a high-density gas state and considering the effect of the interatomic potential on all atoms at once using the density wave approach in reciprocal space.[3,24,25] Based on the idea of the pseudopotential,[26,27] we present a full account of the theory. We show that the minimum in the pseudopotential in reciprocal space drives the liquid to the density wave state. However, the long-range density wave state is incompatible with the SRO, and in our scheme, the competition and compromise between the driving force to form the density wave and the driving force to create better SRO produce the structure with the MRO. We begin by summarizing the nature of the medium-range order, as discussed in our previous publications, introduce the density wave theory and the concept of the pseudopotential, point out that the minimum of the pseudopotential drives the system to the density wave state, demonstrate that the simple density wave state approximately reproduces the density profile, and discuss the implications of the results in relation to dynamic cooperativity. Some details are delegated to the appendices. For simplicity, we primarily focus on simple liquids with spherical interatomic potentials, such as metallic liquids.

II. NATURE OF THE MEDIUM-RANGE ORDER IN LIQUID

The MRO is characterized by fairly regular oscillations of the PDF of which the amplitude attenuates with the distance as

$$|g(r) - 1| \approx \frac{\exp\left(-r/\xi_s(T)\right)}{r}, \tag{4}$$

where $\xi_s(T)$ is the structural coherence length. The process of determining the PDF by experiment through the Fourier-transformation of $S(Q)$ is non-trivial, often compromised by termination errors originating from the limited range of Q in diffraction measurement.[6] For this reason, the MRO has not received sufficient attention it deserves. However, advances in instrumentation, including the use of synchrotron radiation and electrostatic liquid levitation, significantly improved the accuracy of the PDF measurement, and the MRO following Eq. (4) was found to extend much beyond several neighbor shells.[28–32] For instance, the PDF of $Pd_{42.5}Ni_{7.5}Cu_{30}P_{20}$ alloy liquid was found to have strong oscillations reaching beyond 20 Å, as shown in Fig. 1(a), despite its complex chemistry.[32]

It was found that $\xi_s(T)$ is closely related to the dynamic properties of liquid such as viscosity[32] and fragility.[33] The fragility coefficient,

$$m = \left.\frac{d\log\eta(T)}{d(T_g/T)}\right|_{T=T_g}, \tag{5}$$

where $\eta(T)$ is the viscosity, characterizes how quickly viscosity changes with temperature just above T_g.[34] It was found that for a variety of liquids, m is proportional to the number of atoms in the coherence volume at T_g, $n_c = \rho_0(\xi_s(T_g))^3$.[33] Because n_c is a measure of the number of atoms that are correlated with each other, this relationship suggests a direct link between liquid fragility and liquid cooperativity.

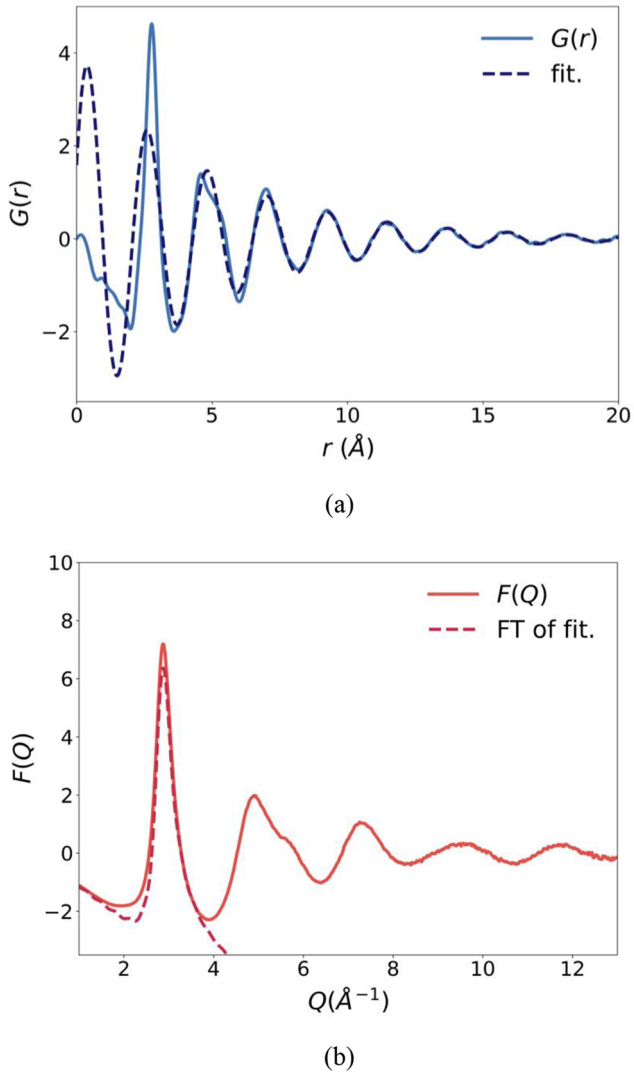

FIG. 1. (a) $G(r) = 4\pi r\rho_0[g(r) - 1]$ of $Pd_{42.5}Ni_{7.5}Cu_{30}P_{20}$ alloy liquid at $T = 573$ K (solid curve) and the fit by Eq. (8) with $A_{MRO} = 1.619$, $Q_1 = 2.835$ Å^{-1}, $\delta_{MRO} = 0.402$, and $\xi_s = 4.743$ Å (dashed curve); (b) $F(Q) = Q[S(Q) - 1]$ of the same liquid (solid curve) and the Fourier-transformation of Eq. (8) shown as $F(Q)$ (dashed curve).

Moreover, $\xi_s(T)$ was found to obey the Curie–Weiss law for temperature dependence above T_g,

$$\frac{\xi_s(T)}{a} = C\frac{T_g}{T - T_{IG}} \quad (T > T_g), \tag{6}$$

where T_{IG} is the ideal glass temperature and $\xi_s(T)$ diverges in extrapolation and is negative for all metallic liquids we studied.[32,35] Below T_g, the structure is frozen, and $\xi_s(T)$ remains constant. We explained this temperature dependence[36] in terms of local density fluctuations away from the structurally coherent glass (SCG) state as

$$G_0(r) = G(r)\exp(r/\xi_s(T)), \tag{7}$$

where

$$G(r) = 4\pi r\rho_0[g(r) - 1]. \tag{8}$$

This state is an imaginary state, which is never achieved because T_{IG} is negative and the structure freezes at T_g.[32] This state is characterized by long-range density waves, although there is no periodicity in the atomic positions. However, the Curie–Weiss law, Eq. (6), implies that there is a driving force to increase local order and approach this state as temperature is lowered. The purpose of the present work is to discuss the origin of this driving force toward the SCG state in terms of formation of density waves. At present, the increase in cooperativity is explained mainly in terms of mode-coupling,[37–39] jamming,[40,41] or random-first-order transition.[42–45] The present work explores another angle to see this phenomenon through energetics rather than through dynamics or geometry.

Ornstein and Zernike (OZ) proposed a scheme to connect the SRO to the MRO through a self-consistency equation and predicted Eq. (4).[46] Slightly different approaches were suggested later by others,[3,47,48] but all these approaches are based on the idea that the MRO is a direct consequence of the SRO. However, as we discussed above and elsewhere,[21,33,35] there are fundamental differences in nature between the SRO and the MRO. Even though the SRO and the MRO are related, they are sufficiently distinct so that the behavior of the MRO cannot be readily predicted from the SRO alone. In the OZ theory, $h(\boldsymbol{r})$, which describes the MRO, is given as a convolution $c(\boldsymbol{r})$, which describes the SRO. However, upon Fourier-transformation to the reciprocal space, a convolution becomes a product, so $h(\boldsymbol{q})$ is non-linearly but directly related to $c(\boldsymbol{q})$. Consequently, the freezing of the MRO at T_g results in the freezing of the SRO in the OZ theory. The mean-field approximation used in the OZ theory is justifiable at high temperatures. However, in the supercooled state, atoms are dynamically correlated and cooperative,[3] and the accuracy of predicting the MRO by the OZ theory is questionable. For example, it predicts the Curie–Weiss behavior, Eq. (6), in high-temperature approximation, but with a positive T_{IG}.[49] Furthermore, Eq. (4) can be explained by the same argument used in explaining Eq. (3).[50] Thus, even though Eq. (4) was first derived by OZ theory based on their equation, the validity of Eq. (4) does not justify the OZ theory.

As shown in Fig. 1(a), for a simple liquid, the oscillations in the PDF representing the MRO are approximately described by

$$g(r) - 1 \approx A_{MRO}\frac{a}{r}\sin(Q_{MRO}r + \delta_{MRO})\exp\left(-\frac{r}{\xi_s}\right), \quad r > r_{cutoff}, \tag{9}$$

where A_{MRO} is the amplitude of the MRO oscillations, δ_{MRO} is the phase factor, which is small, and r_{cutoff} is the position of the first minimum of the PDF beyond the first peak.[50] The MRO wavevector, Q_{MRO}, is very close to the position of the first peak of $S(Q)$, Q_1. As pointed out by Cargill,[20] this is because the first peak of $S(Q)$ is largely determined by the MRO oscillations, as shown in Fig. 1(b). These MRO parameters describe the state of coarse-grained density fluctuations. Therefore, the MRO in the structure may be better described in terms of density waves, represented by local density,

$\rho(\boldsymbol{r})$, and its Fourier-transform, $\rho(\boldsymbol{q})$,[24,25] rather than by the detailed individual atomic positions. Note that the height of the second peak is described well by Eq. (9). However, it contains two subpeaks, and their positions do not agree with the peak by Eq. (9). These subpeaks represent the topological MRO[14–16] as an extension of the SRO, and their positions show temperature dependence similar to that of the first peak by becoming shorter with increasing temperature.[17,18] Thus, the second peak of the PDF is mixed in character, with its height representing the MRO and its peaks representing the extended SRO.

Conversely, the oscillations in $S(Q)$ at high-Q can be approximated by

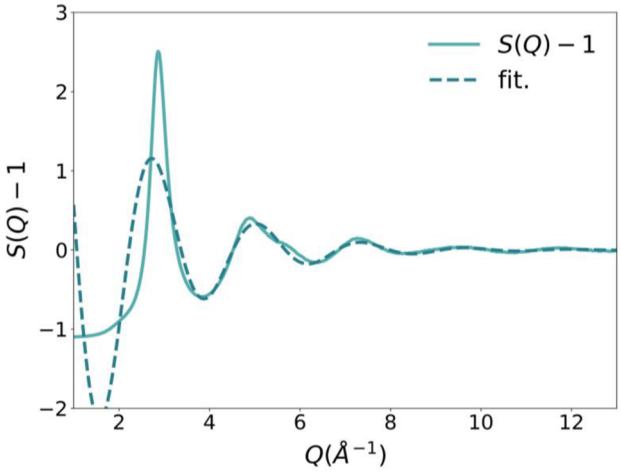

(a)

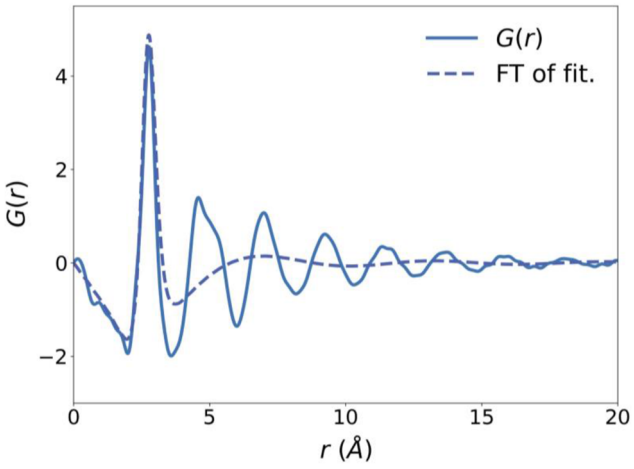

(b)

FIG. 2. (a) $S(Q)$ of $Pd_{42.5}Ni_{7.5}Cu_{30}P_{20}$ alloy liquid at T = 573 K (solid curve) and the fit by Eq. (10) with B_{SRO} = 5.151 Å^{-1}, r_1 = 2.727 Å, δ_{SRO} = 0.224, and κ_s = 1.844 Å^{-1} (dashed curve); (b) $G(r)$ of the same liquid (solid curve) and the Fourier-transformation of Eq. (10) (dashed curve).

$$S(Q) - 1 \approx \frac{B_{SRO}}{Q} \sin\left(Qr_1 + \delta_{SRO}\right) \exp\left(-\frac{Q}{\kappa_s}\right), \quad Q > Q_{cutoff}, \quad (10)$$

where r_1 is the position of the first peak in $g(r)$ and Q_{cutoff} is the position of the first minimum in $S(Q)$ beyond the first peak, as shown in Fig. 2(a). The Fourier-transform of Eq. (10) describes the first peak of the PDF quite well, as shown in Fig. 2(b). Often the one-to-one correspondence between Q and r is assumed.[51] However, this is quite dangerous. As shown here, the first peak of $S(Q)$ corresponds to the MRO oscillations, whereas the first peak of the PDF (SRO) is determined by the high Q part of $S(Q)$. This reciprocal relationship between $S(Q)$ and $g(r)$ for the SRO and MRO is the basis for the present theory.

Equation (6) suggests that $\xi_s(T)$ diverges at T_{IG} and the system reaches the structurally coherent glass (SCG) state with long-range correlation without positional order. Although such a state can never be reached in reality, it proves that there is a force to drive the liquid to such a state at low temperatures. The $S(Q)$ of the SCG state has a δ-function at Q_{MRO}.[32] The three-dimensional $S(\boldsymbol{Q})$ is characterized by a Bragg sphere with a radius of Q_{MRO}. Interestingly, we were able to create a model with such features using the Reverse Monte-Carlo (RMC) method[52] on the $G_0(r)$ obtained by Eq. (7) using the experimentally determined $G(r)$ for the $Pd_{42.5}Ni_{7.5}Cu_{30}P_{20}$ alloy liquid.[32] In the present work, we explain why the SCG state obtained by extrapolation is energetically preferred. We use the density wave theory to discuss the origin of the driving force toward this state.

III. DENSITY WAVE PICTURE OF THE LIQUID STRUCTURE

A. Density wave theory and pseudopotential

We will describe the structure in terms of local density, $\rho(\boldsymbol{r})$, and its Fourier-transform, $\rho(\boldsymbol{q})$, as[24,25,53]

$$\rho(\boldsymbol{r}) = \sum_i \delta(\boldsymbol{r} - \boldsymbol{r}_i) = \int \rho(\boldsymbol{q}) e^{i\boldsymbol{q}\cdot\boldsymbol{r}} d\boldsymbol{q}, \quad (11)$$

$$\rho(\boldsymbol{q}) = \frac{1}{(2\pi)^3} \int \rho(\boldsymbol{r}) e^{-i\boldsymbol{q}\cdot\boldsymbol{r}} d\boldsymbol{r}. \quad (12)$$

$\rho(\boldsymbol{q})$ describes the density waves and is related to the structure function, $S(\boldsymbol{q})$, by

$$S(\boldsymbol{q}) = \frac{1}{\rho_0 V} |\rho(\boldsymbol{q})|^2, \quad (13)$$

where V is the system volume. For simplicity, we consider a liquid in which atoms are interacting with a spherical interatomic potential, $\phi(r)$. The total potential energy is

$$U = \int \rho(\boldsymbol{r}) \rho^*(\boldsymbol{r}') \phi(|\boldsymbol{r} - \boldsymbol{r}'|) d\boldsymbol{r} d\boldsymbol{r}' = \int |\rho(\boldsymbol{q})|^2 \phi(|\boldsymbol{q}|) d\boldsymbol{q}, \quad (14)$$

where

$$\phi(|\boldsymbol{q}|) = \phi(q) = \int \phi(|\boldsymbol{r}|) e^{-i\boldsymbol{q}\cdot\boldsymbol{r}} d\boldsymbol{r}. \quad (15)$$

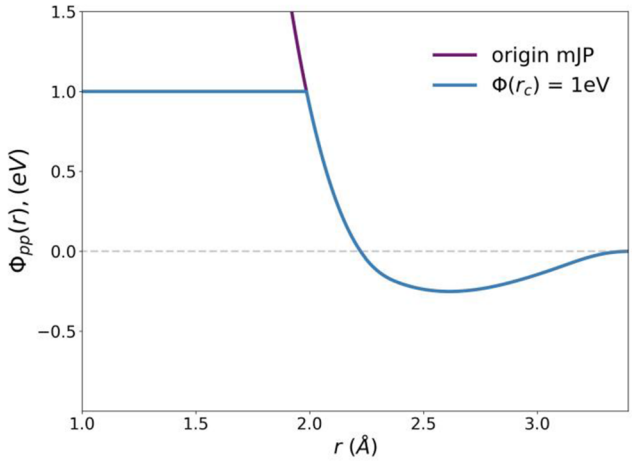

FIG. 3. Modified Johnson potential (mJP) and $\phi_{pp}(r)$ of Fe with $\phi(r_c) = 1$ eV.

The $\phi(r)$ of Fe, the modified Johnson potential,[54] is shown in Fig. 3. It has a minimum at $r_{\min} = 2.62$ Å, which is in close vicinity to the position of the first peak of the PDF, r_1. On the other hand, the $\phi(q)$ of Fe shows no minimum. However, this is misleading because the $\phi(q)$ is dominated by the highly repulsive part of $\phi(r)$, whereas the strongly repulsive part of the potential has no real effect on the total energy because atoms cannot come so close to each other. For this reason, we split the potential into two parts,

$$\phi(r) = \phi_{pp}(r) + \phi_R(r). \tag{16}$$

Here, $\phi_{pp}(r)$ is the "pseudopotential" in which the strongly repulsive part of $\phi(r)$ is removed and $\phi_{pp}(r) = \phi(r_c)$ for $r < r_c$ is assumed[26,27] (Fig. 3). The cutoff, r_c, is chosen such that the cutoff temperature, $k_B T_u = \phi(r_c)$ is well above the actual temperature, and no pair of atoms is found at distances at $r < r_c$ (see Appendix A). $\phi_R(r)$ is the repulsive part of the potential below r_c. Then the total potential energy is

$$U = U_{pp} + U_R, \tag{17}$$

$$U_{pp} = \int \rho(\boldsymbol{r})\rho^*(\boldsymbol{r}')\phi_{pp}(|\boldsymbol{r}-\boldsymbol{r}'|)d\boldsymbol{r}d\boldsymbol{r}' - U_{pp,self}, \tag{18}$$

$$U_R = \int \rho(\boldsymbol{r})\rho^*(\boldsymbol{r}')\phi_R(|\boldsymbol{r}-\boldsymbol{r}'|)d\boldsymbol{r}d\boldsymbol{r}' - U_{R,self}. \tag{19}$$

Because $\phi(r)$ is defined between distinct atoms, we have to subtract the self-energies, $U_{pp,\text{self}}$ and $U_{R,\text{self}}$,

$$U_{pp,self} = \int \rho(\boldsymbol{r})\rho^*(\boldsymbol{r}')W(|\boldsymbol{r}-\boldsymbol{r}'|)\phi_{pp}(|\boldsymbol{r}-\boldsymbol{r}'|)d\boldsymbol{r}d\boldsymbol{r}', \tag{20}$$

$$U_{R,self} = \int \rho(\boldsymbol{r})\rho^*(\boldsymbol{r}')W(|\boldsymbol{r}-\boldsymbol{r}'|)\phi_R(|\boldsymbol{r}-\boldsymbol{r}'|)d\boldsymbol{r}d\boldsymbol{r}', \tag{21}$$

where

$$W(z) = \begin{cases} 1, & if\ z < R_{eff} = a/2, \\ 0, & if\ z \geq R_{eff}, \end{cases} \tag{22}$$

which defines the volume occupied by the central atom. Now, the ground state structure is determined by minimizing U. However, because no pair of atoms is found at distances $r < r_c$ where $\phi_R(r)$ is non-zero, $U_R = 0$. Thus, it is sufficient to minimize U_{pp} to determine the structure. This is equivalent to neglecting the high-energy, unreachable parts of the potential energy landscape (PEL)[4,55] from consideration because they are irrelevant in practice. For this purpose, we divide $\rho(\boldsymbol{r})$ also into two parts,

$$\rho(\boldsymbol{r}) = \rho_{pp}(\boldsymbol{r}) + \rho_R(\boldsymbol{r}), \tag{23}$$

where $\rho_{pp}(\boldsymbol{r})$, the pseudo-density function, is chosen to minimize U_{pp}, whereas $\rho_R(\boldsymbol{r})$ is chosen to enforce $U_R = 0$.

Interestingly, if the strongly repulsive part of the potential is removed, the pseudopotential expressed in q-space, $\phi_{pp}(q)$,

$$\phi_{pp}(q) = \phi_{pp}(|\boldsymbol{q}|) = \int \phi_{pp}(|\boldsymbol{r}|)e^{-i\mathbf{q}\cdot\boldsymbol{r}}d\boldsymbol{r} \tag{24}$$

shows a deep minimum at $q_{\min}$, as shown in Fig. 4 for the modified Johnson potential with various cut-off energies, even though the original $\phi(q)$ has no minimum in the relevant range of q. If $\phi_{pp}(q)$ has a minimum at $\boldsymbol{q}_{\min}$, U_{pp}, and thus the potential energy U, is minimized by

$$\rho_{\min}(\boldsymbol{q}) = \rho_0\delta(\boldsymbol{q}-\boldsymbol{q}_{\min}), \quad \rho_0 = \frac{1}{V}\int \rho(\boldsymbol{r})d\boldsymbol{r}. \tag{25}$$

This state is a long-range density wave state with $\boldsymbol{q}_{\min}$, akin to the structurally coherent glass (SCG) state. Of course, to minimize the total energy, the density waves with high-qs have to be involved as well, but the first minimum is so dominant in $\phi_{pp}(q)$ that in the first order, we just need to consider minimizing the energy within the first valley of $\phi_{pp}(q)$, corresponding to the first peak in $S(q)$. The value of $q_{\min}$ depends only weakly on r_c, as shown in Fig. 5. At $\phi(r_c) = 4.5$ eV, $q_{\min}$ agrees with the wavevector for the structurally coherent glass of Fe $Q_{MRO} = 3.00$ Å^{-1}, obtained by fitting Eq. (8) to the PDF at T_g, and with the position of the first peak of $S(Q)$,

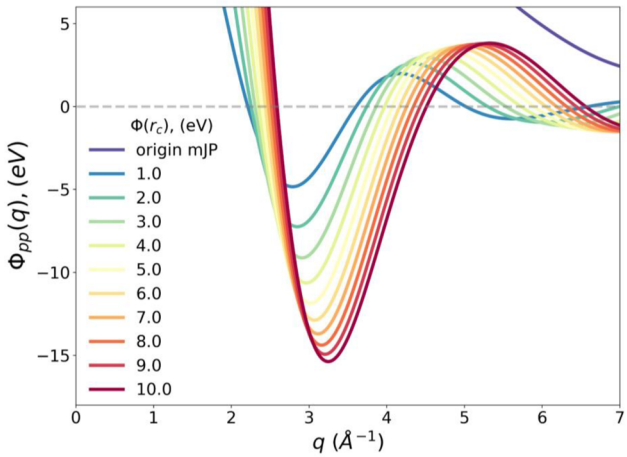

FIG. 4. $\phi(q)$ and $\phi_{pp}(q)$ of Fe with various cut-off values.

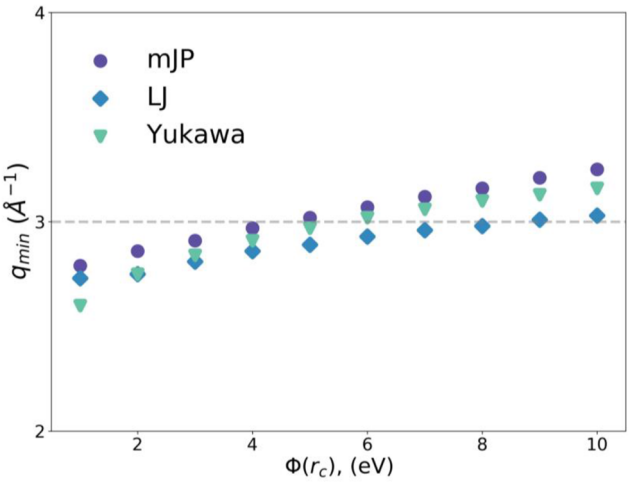

FIG. 5. Dependence of $q_{\min}$ on $\phi(r_c)$ for various potentials. The dashed line represents Q_{MRO}.

$Q_1 = 3.02$ Å^{-1}. Therefore, it is reasonable to speculate that $\phi_{pp}(q)$ is driving the system to the structurally coherent glass state. Q_1 and r_1 are connected through the formula,[20] $Q_1 r_1 \approx 5\pi/2$, reflecting the position of the first peak in Eq. (9). Often the one-to-one correspondence between Q and r is assumed.[51] However, this is highly misleading because the first peak of $S(Q)$ corresponds to the MRO oscillations whereas the first peak of the PDF affects the higher Q part of $S(Q)$, as shown in Figs. 1 and 2.[20,50] Therefore, it is most likely that the minimum in $\phi_{pp}(q)$ is providing the driving force to form the SCG state. The actual ground state is determined usually with additional constraints, such as keeping the total number of atoms constant. Such constraints result in Lagrangian multipliers for minimization of the potential energy. In addition, we have to consider the effect of $\phi_{pp}(q)$ at higher q beyond the first valley. These details are left for future study.

To examine the generality of the idea that the SCG state is driven by the first minimum of $\phi_{pp}(q)$, we studied $\phi_{pp}(q)$ for two other simple pairwise potentials, the Lennard-Jones (LJ) potential and the repulsive Yukawa (Y) potential. In both cases, the parameters were chosen such that the atomic number density, Q_1, and the potential depth, $\phi_{pp}(Q_1)$, agree with those of liquid Fe (see Appendix B). As shown also in Fig. 5, the value of $q_{\min}$ was found to be close to Q_1 and only weakly dependent on $\phi(r_c)$ for both cases. This applies even to the hard-sphere model.[27] Therefore, it is likely that in DRP liquids in general, the structurally coherent glass state is driven by $\phi_{pp}(q)$.[26] Instead of focusing on $\phi(r)$ in real space directly affecting two atoms at a time as in the bottom-up approach, we consider the effect of $\phi_{pp}(q)$ operating on the entire system of atoms in the high-temperature gaseous state in the top-down approach in reciprocal space. Then, the minimization of the potential energy in Eq. (24) by forming the density wave state is likely be the force to drive the liquid toward the structurally coherent glass state. The presence of this substantial driving force toward the density wave state explains why the well-defined oscillations characterizing the MRO persist up to long distances and high temperatures even for metallic alloy liquids with complex compositions.

B. Density wave state

The structurally coherent glass (SCG) state is macroscopically isotropic and cannot be described by a single density wave, Eq. (24). To describe this state approximately, we consider the density wave (DW) state defined by a large set of density wave vectors $\boldsymbol{q}_{DW}$ with the same length, $q_{DW} = |\boldsymbol{q}_{DW}| = Q_{MRO}$, evenly distributed over all angles in $\boldsymbol{q}$ space forming a Bragg sphere and use it as the pseudo-density function,

$$\rho_{pp}(\boldsymbol{r}) = \rho_{DW,\Lambda}(\boldsymbol{r}) = \rho_0 + \int \rho_\Lambda(\boldsymbol{q}_{DW}) e^{i\boldsymbol{q}_{DW}\cdot\boldsymbol{r}} d\boldsymbol{q}_{DW}, \quad (26)$$

where

$$\rho_\Lambda(\boldsymbol{q}_{DW}) = |\rho_\Lambda(\boldsymbol{q}_{DW})| e^{i\delta_{DW,\Lambda}(\boldsymbol{q}_{DW})}. \quad (27)$$

To keep the density real, we assume

$$|\rho_\Lambda(-\boldsymbol{q}_{DW})| = |\rho_\Lambda(\boldsymbol{q}_{DW})|, \quad \delta_{DW,\Lambda}(\boldsymbol{q}_{DW}) = -\delta_{DW,\Lambda}(-\boldsymbol{q}_{DW}). \quad (28)$$

The phase factor, $\delta_{DW,\Lambda}(\boldsymbol{q}_{DW})$, is added to avoid atom pileups. It varies strongly and nearly randomly for the $\boldsymbol{q}_{DW}$ vectors in different directions. The sets of the phase factors, $\{\delta_{DW,\Lambda}(\boldsymbol{q}_{DW})\}$, and amplitudes, $\{|\rho_\Lambda(\boldsymbol{q}_{DW})|\}$, characterize each density wave state. For simplicity, we use $\boldsymbol{\Lambda}$ to designate the sets of the phase factors, $\{\delta_{DW,\Lambda}(\boldsymbol{q}_{DW})\}$, and amplitudes, $\{|\rho_\Lambda(\boldsymbol{q}_{DW})|\}$. Because there are infinite sets of these factors, there are infinite density wave states, $\rho_{DW,\Lambda}(\boldsymbol{r})$. The DW state has long-range density correlations without translational symmetry. A quasicrystal[56] is an example of a solid with long-range correlation without translational symmetry. It is a crystal in six-dimensions projected to three-dimensions with an irrational projection angle.[57] The DW state is a crystal in N-dimensions projected with nearly random phase factors because the Bragg sphere can be considered to be made of an infinite number of Bragg points covering the sphere. Below, we show that the DW state, described by the pseudo-density function $\rho_{pp}(\boldsymbol{r})$, is close to the structurally coherent glass state of liquid except for details of the SRO.

The $S(q)$ of the structure defined by Eq. (26) has just the Bragg peak at q_{DW}, which is the first peak of the $S(q)$ of the SCG state. Because the first peak of $S(q)$ describes the MRO as shown in Fig. 1, the PDF of this state represents just the MRO portion of the PDF,

$$g_{MRO}(r) - 1 = B_\rho(q_{DW}) \frac{{q_{DW}}^2}{\pi\rho_0^2} \frac{\sin q_{DW} r}{q_{DW} r}, \quad (29)$$

where

$$B_\rho(q_{DW}) = L^2 \left\langle |\rho(\boldsymbol{q}_{DW})|^2 \right\rangle \quad (30)$$

and $V = L^3$. Its derivation is given in Appendix C. The total potential energy, Eq. (14), is independent of the phase factors. Thus, all the density wave states characterized by the sets of different phase factors are degenerate in energy for a given value of $B_\rho(q_{IG})$. This basic degeneracy is reflected in the high degeneracy of the basins in the PEL.[4,55] The PDF predicted by Eq. (30) agrees well with the MRO portion of the PDF, as shown in Fig. 6 by the dashed curve. Thus, the DW state approximately represents the principal density fluctuations in the SCG state.

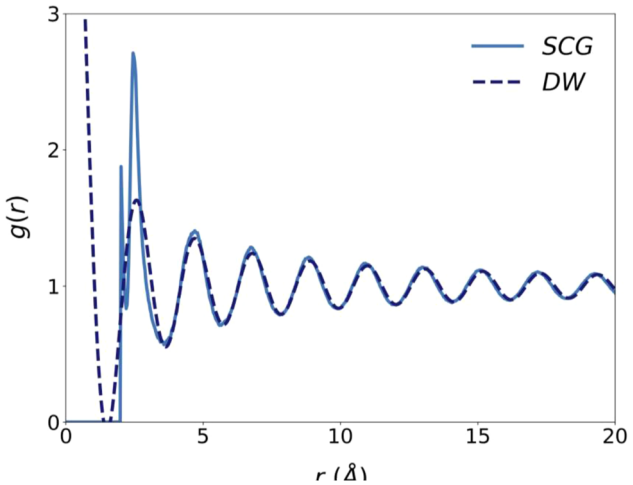

FIG. 6. PDF of the model of the structurally coherent glass (SCG) state for liquid Fe created by the RMC method (solid curve). The sharp peak at 2.0 Å reflects the imposed minimum atomic distance. See Ref. 32 for details of the model. The dashed curve represents the density wave (DW) state given by Eq. (28).

However, the wavelength of this density wave in liquid Fe, $\lambda_{DW} = 2\pi/q_{DW} = 2.09$ Å, is too long to specify the atomic position with sufficient accuracy. In addition, because $\phi(r)$ is repulsive at short distances, $\rho(\boldsymbol{r})$ has gaps between atoms where $\rho(\boldsymbol{r}) = 0$. The pseudo-density function, $\rho_{pp}(\boldsymbol{r})$, cannot accurately describe these atomic level details, even though it catches the principal density fluctuations. To describe the atomic positions and these gaps accurately, we need to include $\rho_R(\boldsymbol{r})$, which represents contributions from waves with $\boldsymbol{qs}$ higher than $q_{\rm IG}$ and eliminates atomic overlaps. Indeed, as shown in Fig. 6, the $G(r)$ of the DW state badly misses the first peak for the SCG state in height and sharpness. The sharp and tall first peak in $G(r)$, seen in Figs. 1(a) and 6, indicates good SRO, which is driven by $\phi(r)$ in real space. Thus, the DW state driven by $\phi_{pp}(q)$ in q space and the SRO driven by $\phi(r)$ in real space are mutually incompatible. As we discuss below, the conflict between these two competing driving forces determines the extent of the MRO.

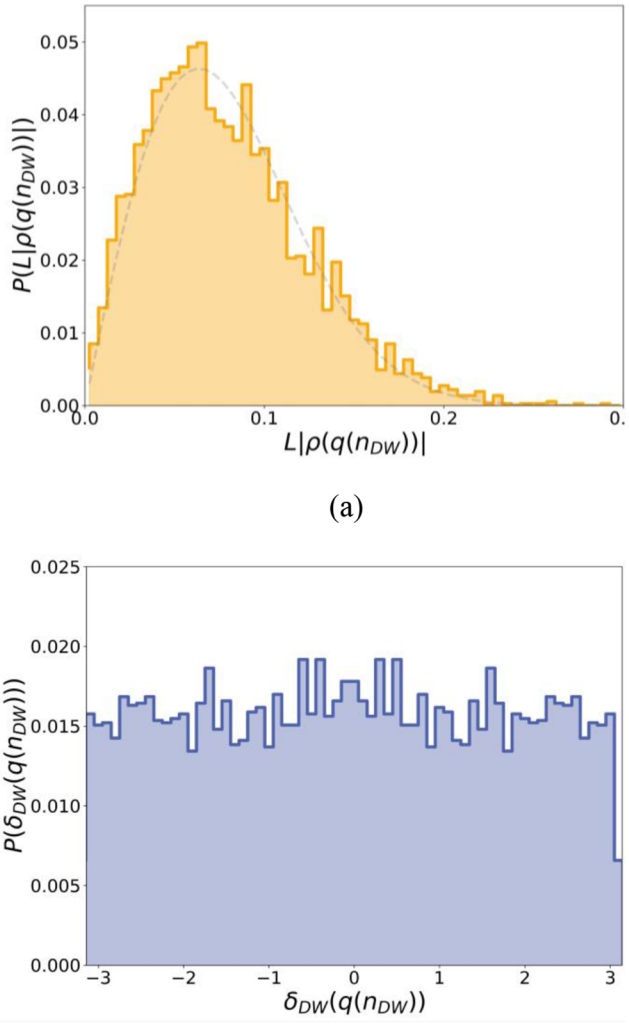

FIG. 8. Distribution of values of (a) $L|\rho(\boldsymbol{q}(\boldsymbol{n}_{DW}))|$ and (b) $\delta_{DW}(\boldsymbol{q}(\boldsymbol{n}_{DW}))$. The dashed curve in (a) represents Eq. (33).

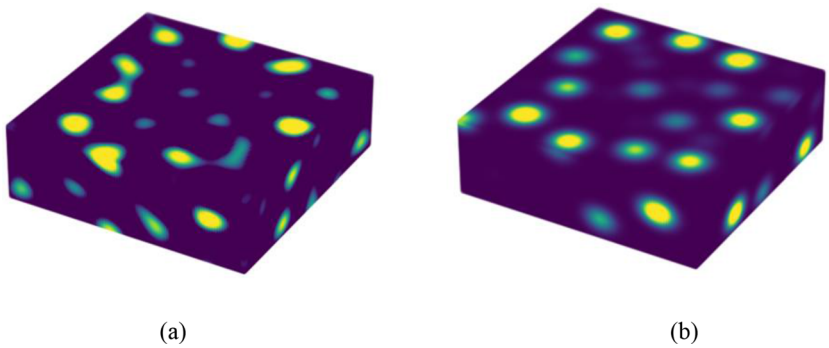

FIG. 7. (a) Density profile of $\rho_{DW}(\boldsymbol{r})$ by Eq. (26) compared with (b) that of the model, $\rho_{model}(\boldsymbol{r})$.

To test this density wave picture, we start with the model of the structurally coherent glass state created by the RMC method based on the structure of liquid Fe, the PDF of which is shown in Fig. 6. The original model consists of 54 000 atoms in a supercell of L_s^3 (L_s = 88.3 Å) with cubic periodic boundary conditions and the constraint of a minimum atomic distance of 2.0 Å. However, because the cubic boundary conditions are inconsistent with the assumed isotropic nature of the density wave model, the model could not maintain correlation over the whole volume and the oscillations in $G(r)$ decayed beyond 50 Å. Thus, we took a central cubic portion of the model with L = 50 Å for the analysis of the structure and the PDF. The allowed $\boldsymbol{q}$ vectors are $\boldsymbol{q_n} = \Delta q\boldsymbol{n}$, where $\boldsymbol{n} = (n_x, n_y, n_z)$, where $\Delta q = 2\pi/L$ and n_x, n_y, and n_z are integers. $\boldsymbol{q}(\boldsymbol{n_{DW}}) = \Delta q\boldsymbol{n_{DW}}$ is chosen so that

$$\left(n(q_{DW}) - \frac{1}{2}\right)^2 < n_{DW}^2 < \left(n(q_{DW}) + \frac{1}{2}\right)^2, \quad n(q_{DW}) = \frac{q_{DW}}{\Delta q}. \tag{31}$$

Then, the density is given by

$$\rho_{DW}(\boldsymbol{r}) = \rho_0 + \sum_{\boldsymbol{n}_{DW}} |\rho(\boldsymbol{q}(\boldsymbol{n}_{DW}))| e^{i(\boldsymbol{q}(\boldsymbol{n}_{DW})\cdot\boldsymbol{r} + \delta_{DW}(\boldsymbol{q}(\boldsymbol{n}_{DW})))}. \tag{32}$$

The density profile of $\rho_{DW}(\boldsymbol{r})$ by Eq. (32) compares well except for details with that of the model, $\rho_{model}(\boldsymbol{r})$, as shown in Fig. 7. $\rho_{model}(\boldsymbol{r})$, initially composed of δ-functions, is convoluted with a Gaussian profile with width w (=0.4 Å) to model the uncertainty in position, which is of the order of $\lambda_{IG}/2$, and mitigate the need of higher q contributions. As indicated by Eqs. (29) and (30), the values of $|\rho(\boldsymbol{q}(\boldsymbol{n}_{DW}))|$ scale as L^{-1}. The $L|\rho(\boldsymbol{q}(\boldsymbol{n}_{DW}))|$ shown in Fig. 8(a) is widely distributed in magnitude, with the approximate probability of the two-dimensional Gaussian distribution reflecting the two-dimensional nature of the Bragg sphere,

$$P(L|\rho(\boldsymbol{q}(\boldsymbol{n}_{DW}))|) = \frac{L|\rho(\boldsymbol{q}(\boldsymbol{n}_{DW}))|}{2\pi\sigma_{\rho(q)}^2} \exp\left(-\frac{L^2|\rho(\boldsymbol{q}(\boldsymbol{n}_{DW}))|^2}{2\sigma_{\rho(q)}^2}\right). \tag{33}$$

The phase factor, $\delta_{DW}(\boldsymbol{q}(\boldsymbol{n}_{DW}))$, is evenly distributed from $-\pi$ to π, as shown in Fig. 8(b).

IV. DENSITY WAVES IN REAL LIQUID AND GLASS

Whereas the DW state is the lowest energy state formed at the minimum of $\phi(q)$, at finite temperature, the system deviates from the DW state because of thermal excitation. In addition, there are geometrical frustration effects, as we discuss below. Consequently, structural coherence cannot fully develop in liquid and glass, and the density wave oscillations in the PDF are exponentially attenuated, indicating limited spatial coherence, following Eq. (9). Whereas the DW state has a Bragg-like first peak in $S(Q)$, real liquid and glass have a broader first peak due to limited coherence. When the attenuation is purely exponential, the shape of the first peak of $S(Q)$ is Lorentzian.[50] We now discuss how thermal and geometrical effects limit the structural coherence in liquid and glass.

A. Thermal excitation

In crystals, thermally excited phonons have well-defined wavevectors, $\boldsymbol{q}$, so that the lattice periodicity is not affected by phonon excitation. As a result, the Bragg peaks in $S(Q)$ remain δ-function-like, and only their heights are reduced by the Debye–Waller factor.[6] In contrast, phonons in liquid are strongly attenuated by disorder,[1–3] and local density fluctuations are poorly correlated in space. In addition, non-phonon, topological excitations dominate at high temperatures.[58–61] Consequently, the structure itself fluctuates, resulting in spatially limited structural coherence.

In Ref. 36, the temperature dependence of the MRO coherence length, $\xi_s(T)$, was explained in terms of local atomic-level pressure (density) fluctuations. It can be shown that $\xi_s(T)$ is related to the local atomic-level volume fluctuations through

$$\frac{a}{\xi_s} = \frac{10\pi^3}{9}\left\langle\left(\varepsilon_V^R\right)^2\right\rangle, \tag{34}$$

where ε_V^R is the relaxation volume strain in the Eshelby theory[62] of local geometrical mismatch between an inclusion and a hole in the matrix, and it has two components,

$$\left\langle\left(\varepsilon_V^R\right)^2\right\rangle = \left\langle\left(\varepsilon_V^{R,mf}\right)^2\right\rangle + \left\langle\left(\varepsilon_V^{R,th}\right)^2\right\rangle, \tag{35}$$

where $\varepsilon_V^{R,th}$ is the thermal strain and $\varepsilon_V^{R,mf}$ is the atomic misfit strain. The thermal strain is related to the atomic-level pressure p_i[63] by

$$\varepsilon_V^{R,th} = (K_\alpha - 1)\frac{p_i}{B}, \tag{36}$$

where B is bulk modulus and

$$K_\alpha = \frac{3(1-\nu)}{2(1-2\nu)}, \tag{37}$$

where ν is Poisson's ratio. The atomic-level pressure averages out to zero so that $\langle p\rangle = 0$, but it has a wide Gaussian distribution, with the second moment following the equipartition theorem,[64,65]

$$\langle p^2\rangle = \frac{k_B T}{2BVK_\alpha}. \tag{38}$$

Thus,

$$\left\langle\left(\varepsilon_V^{R,th}\right)^2\right\rangle = \frac{(K_\alpha - 1)^2}{K_\alpha}\frac{k_B T}{2BV}. \tag{39}$$

Now, $\varepsilon_V^{R,mf}$, the atomic misfit strain, originates from structural frustration, as discussed below. Thus, the MRO coherence length is given by the Curie–Weiss equation,

$$\begin{aligned}\left\langle\left(\varepsilon_V^R\right)^2\right\rangle &= \left\langle\left(\varepsilon_V^{R,mf}\right)^2\right\rangle + \left\langle\left(\varepsilon_V^{R,th}\right)^2\right\rangle \\ &= \frac{9}{10\pi^3}\frac{a}{\xi_s} = \frac{(K_\alpha - 1)^2}{K_\alpha}\frac{k_B(T - T_{IG})}{2BV},\end{aligned} \tag{40}$$

where

$$\left\langle\left(\varepsilon_V^{R,mf}\right)^2\right\rangle = -\frac{(K_\alpha - 1)^2}{K_\alpha}\frac{k_B T_{IG}}{2BV}. \tag{41}$$

This theory explains the temperature dependence of $\xi_s(T)$ with excellent quantitative accuracy with the only adjustable value of $\varepsilon_V^{R,mf}$, which cannot be theoretically calculated.[36]

B. Conflict between SRO and density wave state

The first peak of $g_{MRO}(r)$ in the density wave state calculated by Eq. (29) is as wide as the second peak (Fig. 6, dashed curve). Such a broad peak is not compatible with $\phi(r)$, which prefers the first peak of $g(r)$ to be tall and narrow. As shown in Fig. 6, the first peak of the $g(r)$ of the SCG state is much taller and sharper than that of the DW state, suggesting that the SRO of the SCG state is better than that of the DW state as a result of imposing a minimum in atomic separation in constructing the SCG model. Furthermore, even the model of the SCG state has poor SRO with very diverse local structures exemplified by the probability of the icosahedral clusters below 1%,[32] whereas an icosahedral local structure is strongly preferred in the bottom-up approach.[11–13]

Therefore, it is clear that the driving force to produce the DW state with $q = |\boldsymbol{q}_{DW}|$ by minimizing $\phi_{pp}(q)$ in q space is in conflict with the force to produce the SRO with as small local distortion as possible by minimizing $\phi(r)$ in real space. This conflict between the two driving forces is the origin of the misfit strain, $\varepsilon_V^{R,mf}$, and limits the DW coherence in space, exponentially damping the DW correlation. Again, its spatial average is zero, $\left\langle \varepsilon_V^{R,mf} \right\rangle = 0$, and its second moment determines T_{IG} by Eq. (41). Because the value of T_{IG} is related to fragility,[36] it is suspected that covalency in the atomic bond is its origin. Strong covalency promotes better SRO with well-defined local topology and suppresses the DW formation. It is interesting to note that the atomic size mismatch, the differences in atomic size among the constituent elements, is not related to the DW coherence length.[50] Atomic size mismatch destabilizes the crystalline solid solution and in turn promotes glass formability.[66] However, liquid and glass can accommodate size mismatch by adjusting the local structure.[67] Therefore, chemical atomic size mismatch is not the origin of this effect.

C. Density wave picture of real liquid and glass

Because of thermal excitation and geometrical frustration, the DW coherence is limited in space in liquid and glass. Therefore, real liquid can be considered a collection of a very large number of different DW states, each characterized by a different set, $\boldsymbol{\Lambda}$, confined to a limited volume specified by ξ_s. Then, the density profile of real liquid and glass can be given as an assembly of many DW states by

$$\rho(\boldsymbol{r}) = \sum_{\boldsymbol{\Lambda}} w_{\xi,\boldsymbol{\Lambda}}(\boldsymbol{r},\boldsymbol{r}')\rho_{DW,\boldsymbol{\Lambda}}(\boldsymbol{r}), \tag{42}$$

where $w_{\xi,\boldsymbol{\Lambda}}(\boldsymbol{r},\boldsymbol{r}')$ is a window function with a size factor of ξ, centered at $\boldsymbol{r}'$, for each DW state $\boldsymbol{\Lambda}$. The variation in the base density wave state, $\boldsymbol{\Lambda}$, with position $\boldsymbol{r}'$ represents the fundamental incoherence in the state of real liquid and glass. The window functions can be overlapping in space. In our model, they are strongly overlapping exponentially decaying functions centered on each atom. If $w_{\xi,\boldsymbol{\Lambda}}(\boldsymbol{r},\boldsymbol{r}')$ is the same for all $\boldsymbol{\Lambda}$ and dependent only on $\boldsymbol{r}-\boldsymbol{r}'$. Through the convolution theorem, the Fourier-transform of Eq. (33) is

$$\rho(\boldsymbol{q}) = \sum_{\boldsymbol{\Lambda}} \rho(\boldsymbol{q}_{DW,\boldsymbol{\Lambda}}) W_{\xi,\boldsymbol{\Lambda}}(\boldsymbol{q}-\boldsymbol{q}_{DW}), \tag{43}$$

where $W_{\xi,\boldsymbol{\Lambda}}(\boldsymbol{q})$ is the Fourier-transform of $w_{\xi,\boldsymbol{\Lambda}}(\boldsymbol{r})$. Because $\rho(\boldsymbol{q}_{DW,\boldsymbol{\Lambda}})$ is a δ-function, the peak profile of $\rho(q)$ is determined by $W_{\xi,\boldsymbol{\Lambda}}(\boldsymbol{q})$. Thus, broadening of the first peak of $S(Q)$ can be explained as a result of spatial confinement of the DW state. Then, by examining the shape of the first peak of $S(Q)$, we gain knowledge on the nature of the window function. For many good metallic liquids and glasses with long ξ_s, it is close to the Lorentzian,[50] consistent with the window function and with the exponentially decaying function, whereas it is closer to the Gaussian for liquids and glasses with short ξ_s. The term "ideality" was introduced to indicate the closeness to the Lorentzian shape.[50]

V. DISCUSSION

A. Density wave periodicity

For various metallic liquids studied by simulation,[32] Q_1 approximately shows a linear relation to $\rho_0^{1/3}$, as shown in Fig. 9(a), by

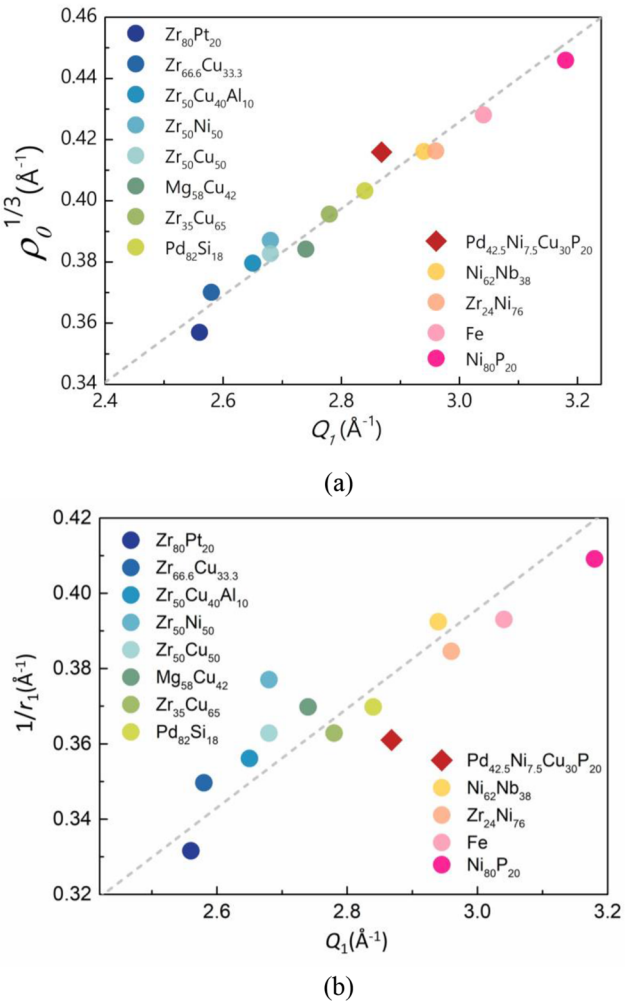

FIG. 9. (a) Plot of $\rho_0^{1/3}$ against Q_1, the first peak position of $S(Q)$, for various metallic liquids by experiment for $Pd_{42.5}Ni_{7.5}Cu_{30}P_{20}$ alloy liquid and by simulation for others. The dashed line represents $Q_1 = C_{MRO}\rho_0^{1/3}$, with $C_{MRO} = 7.04 \pm 0.023$; (b) plot of $1/r_1$ against Q_1, where r_1 is the first peak position of $g(r)$, for the same group of liquids. The dashed line represents $Q_1 = C_{SRO}/r_1$ with $C_{SRO} = 7.58 \pm 0.062$.

$$Q_1 = C_{MRO}\rho_0^{1/3}, \text{ with } C_{\mathrm{MRO}} = 7.04 \pm 0.023. \quad (44)$$

Therefore, the MRO periodicity normalized by $\rho_0^{1/3}$ is nearly universal for metallic liquids with the DRP structure, regardless of details of atomic bonds and interatomic potentials. In Eq. (9), the first peak is at $a_{MRO} = 5\pi/2Q_{MRO} \approx 5\pi/2Q_1$ if we neglect δ_{MRO}. If we assume this distance is twice the effective radius of an atom, R_{eff}, the volume fraction occupied by atoms by assuming a spherical atom, i.e., the atomic packing fraction (PF), is given by

$$PF = \frac{4\pi}{3}\rho_0 R_{eff}^3 = \frac{125\pi^4}{48C_{MRO}^3}, \quad (45)$$

which gives $PF = 0.726$ for the value of C_{MRO} in Eq. (44). This value is very close to that of the *f.c.c.* structure (0.74) and of amorphous Fe (0.745[68]), suggesting that the result in Eq. (44) supports the idea that the DRP liquids have a nearly universal DW periodicity, which depends only on the atomic number density. The position of the first peak of $g(r)$, r_1, is inversely related to Q_1, as shown in Fig. 9(b), through $Q_1 = C_{SRO}/r_1$, with $C_{\mathrm{SRO}} = 7.58 \pm 0.062$. However, the deviation in C_{SRO}, 0.82%, is almost three times larger than that of C_{MRO}, 0.33%. Furthermore, the MRO phase shift in Eq. (9), δ_{MRO}, is not negligible and varies with composition,[19] affecting the PDF peak positions. These results suggest that Q_1 reflects the average structure of the system well, whereas r_1 does a poorer job, contrary to general perception. This is probably because r_1 is influenced by local chemistry and the nature of atomic bonds such as covalency. By comparing $Q_1 r_1$ to density, Ref. 29 concluded that glass structure has a fractal dimension whereas the notion of fractal dimension of the structure was refuted later.[69] The failure of Ref. 29 is most likely because r_1 is not a reliable parameter of the global structure of liquid and glass.

B. Dynamic cooperativity and the MRO

Below the viscosity crossover, or Arrhenius, temperature, T_A, the viscosity of a liquid becomes super-Arrhenius and increases rapidly with decreasing temperature toward the glass transition.[34,60,70,71] Various theories were proposed to explain this rapid rise in viscosity,[1–5,37–45] but the issue is still open. It is widely agreed upon that the rise in viscosity is related to an increase in atomic cooperativity.[71–73] Bouchaud and Biroli[8] and Montanari and Semerjian[73] argued that the activation energy for viscosity in cooperative liquid and glass is proportional to the volume defined by the cooperative regions. Now, the region of atomic cooperativity has long been considered to be a local defect-like region where atomic density is low and atoms are easier to move.[71–80] However, this assumption may need to be scrutinized in light of recent results. In crystalline solids, structural defects provide atomic mobility, and this knowledge prompted the definition of defects in glasses as soft or loose regions. However, there is a critical difference between defects in crystal and those in glass. In crystalline solids, defects are defined in terms of local deviations from the lattice periodicity. When they move, their identity does not change because they are topologically protected. On the contrary, in liquid and glass, defects are not topologically protected and change their structure and nature significantly upon motion. In fact, application of small strain significantly changes the activation energy spectrum for local deformation.[81]

Furthermore, at the saddle point of the PEL, the local structure configurationally melts for a short time (~1 ps)[82] and largely loses the memory of their thermal history.[83] In general, the saddle point is known as a generator of chaos,[84,85] and it is difficult to predict the behavior after passing through the saddle point. Even before the final saddle point is reached, the local PEL surface is far from smooth and shows complex fractal heterogeneity[86,87] because atomic connectivity changes all the time even in the apparently elastic regime.[88,89] These numerous small local saddle points in the PEL can generate chaotic uncertainty, eventually wiping out previous history. Then, a deformation event may indeed be initiated by defects, but the local structure changes significantly during the deformation event so that the actual deformation event may be determined by more general resistance to flow rather than by the initial state of flow.

In the density wave picture, the movements of atoms are described in two ways, through the change in the phase factor, $\delta_{DW}(\boldsymbol{q}_{DW})$ of Eq. (27) (phason)[53] and the change in the amplitude of the density waves, $|\rho(\boldsymbol{q}_{DW})|$ (amplitudon). Because the density wave represents many atoms, a phason or amplitudon excitation created by an atom affects all atoms within the coherence volume, resulting in cooperative atomic dynamics. In other words, density waves provide resistance to atomic motion. This explains why the number of atoms in the coherence volume, $n_c = \rho_0(\xi_s(T))^3$, is a good parameter to control the activation energy of viscosity[32] and fragility.[33]

In this context, the concept of hyperuniformity[90] could provide interesting guidance. Hyperuniformity refers to suppression of density fluctuations by some internal order. It produces rigidity and solid-like behavior. Crystals are a trivial case where the lattice periodicity totally suppresses density fluctuations. In many amorphous systems, hidden order can suppress density fluctuations and results in the hyperuniform state.[91–98] Now, the density wave state discussed here is obviously hyperuniform when it is in equilibrium, and it can be the basis for rigid, glassy behavior, but that state cannot be reached because of the glass transition and the fact that T_{IG} is negative. However, liquid is made of an assembly of many local DW states with limited spatial extension. Then, the idea of hyperuniformity could be expanded to account for local and dynamic behavior, and it could explain resistance to flow by the MRO. Whereas this idea needs further study, it points to a promising direction of research.

VI. CONCLUSION

The conventional approaches to elucidate the atomic structure of liquid and glass are *bottom-up* approaches, in which one starts with focusing on an atom and its neighboring atoms and adds more atoms to form the global structure, locally minimizing the interatomic potential energy. However, with this approach, it is difficult to explain why well-defined MRO oscillations are always observed, even in metallic liquids with complex compositions. It is commonly assumed that the MRO is a direct consequence of the SRO. However, the SRO and MRO are fundamentally different in nature because the SRO describes atomic correlations within the atomic cage whereas the MRO describes correlations with coarse-grained density fluctuations. To resolve this conundrum, we suggest that the MRO is not a direct consequence of the SRO but is driven by a different collective force. We propose a two-way approach composed of an inverted *top-down* approach as well as the bottom-up approach

to conceptualize the formation of the structure. In the top-down approach, we start with a high-density gas state and minimize the global potential energy through density waves, which is driven by the minimum in the pseudopotential in reciprocal space. The two approaches are not mutually compatible, and the competition and compromise between the two driving forces result in a structure with the MRO. The strength of the MRO, which is expressed by the MRO coherence length and is called "ideality," is unrelated to the atomic size mismatch and compositional complexity.[50] It is suspected that the strong driving force for the SRO, such as strong covalency, compromises the MRO. The MRO coherence length is directly related to viscosity near T_g[32] and liquid fragility.[33] We surmise that this is because the MRO, rather than the SRO, provides resistance to flow in supercooled liquid and glass. The even-handed two-way approach proposed here provides a more balanced account of the structure and dynamics in simple liquid and glass. This could form a basis for developing a more realistic and general theory to describe the state of liquid and glass.

ACKNOWLEDGMENTS

The authors thank M. L. Manning, A. Lemaitre, Y. Shinohara, C. K. C. Lieou, and E. Zarkadoula for helpful discussions. This work was supported by the U.S. Department of Energy, Office of Science, Basic Energy Sciences, Materials Sciences and Engineering Division. This work was supported also by the Creative Materials Discovery Program through the National Research Foundation of Korea (NRF) funded by the Korean Government (MSIT) (no. NRF-2023M3D1A107206822) and 2023 Hongik University Research Fund to CWR. This research used resources of the National Energy Research Scientific Computing Center (NERSC), a U.S. Department of Energy Office of Science User Facility located at Lawrence Berkeley National Laboratory, operated under Contract No. DE-AC02-05CH11231 using NERSC Award No. BES-ERCAP0020503. This article has been authored by UT-Battelle, LLC, under Contract No. DE-AC05-00OR22725 with the U.S. Department of Energy. The United States Government retains and the publisher, by accepting the article for publication, acknowledges that the United States Government retains a non-exclusive, paid-up, irrevocable, world-wide license to publish or reproduce the published form of this manuscript, or allow others to do so, for United States Government purposes. The Department of Energy will provide public access to these results of federally sponsored research in accordance with the DOE Public Access Plan (http://energy.gov/downloads/doe-public-access-plan).

AUTHOR DECLARATIONS

Conflict of Interest

The authors have no conflicts to disclose.

Author Contributions

Takeshi Egami: Conceptualization (lead); Formal analysis (lead); Funding acquisition (lead); Investigation (equal); Methodology (lead); Project administration (lead); Supervision (lead); Validation (equal); Writing – original draft (lead); Writing – review & editing (equal). **Chae Woo Ryu**: Data curation (lead); Investigation (equal); Writing – original draft (supporting); Writing – review & editing (equal).

DATA AVAILABILITY

The data that support the findings of this study are available from the corresponding author upon reasonable request.

APPENDIX A: PSEUDOPOTENTIAL

A measure of the magnitude of $k_B T_u = \phi(r_c)$ may be given by the timescale of overcoming the potential,

$$\tau_{pp} = \tau_D \exp\left(\frac{\phi(r_c)}{k_B T}\right), \tag{A1}$$

where τ_D is the Debye time ($\sim 10^{-13}$ s). This should be larger than the total MD run time, τ_{MD}. For liquid Fe at 2000 K and for $\tau_{\mathrm{MD}} = 10^{-9}$ s, $\phi(r_c)$ must be larger than 2 eV.

APPENDIX B: LJ AND YUKAWA POTENTIALS

The Lennard-Jones (LJ) potential,

$$\phi_{LJ}(r) = A\left[\left(\frac{r}{\sigma}\right)^{12} - \left(\frac{r}{\sigma}\right)^{6}\right], \tag{B1}$$

with $A = 0.1$ eV and $\sigma = 2.33$ Å, and the Yukawa potential,

$$\phi_Y(r) = \frac{B}{r}\exp(-\kappa r), \tag{B2}$$

with $B = 10^5$ eV and $\kappa = 5.328$ Å^{-1}, were used in simulation.

APPENDIX C: DENSITY WAVE COEFFICIENT

From Eqs. (11) and (12), for an atomic system,

$$\rho(\boldsymbol{q}) = \sum_i e^{-i\boldsymbol{q}\cdot\boldsymbol{R}_i}. \tag{C1}$$

Thus, the structure function $S(\boldsymbol{q})$ is given by

$$S(\boldsymbol{q}) = \frac{1}{N}\sum_{i,j} e^{-i\boldsymbol{q}\cdot(\boldsymbol{R}_i - \boldsymbol{R}_j)} = \frac{1}{\rho_0 V}|\rho(\boldsymbol{q})|^2. \tag{C2}$$

For a spherical system,

$$S(q) = \langle S(\boldsymbol{q})\rangle = \frac{1}{4\pi}\int S(\boldsymbol{q})d\boldsymbol{\Omega}_q = \frac{1}{\rho_0 V}\langle|\rho(\boldsymbol{q})|^2\rangle. \tag{C3}$$

For a Bragg peak at $q = q_1$, the area of the peak is

$$A_\rho(q_1) = \frac{1}{\rho_0 V}\langle|\rho(\boldsymbol{q}_1)|^2\rangle\Delta q, \tag{C4}$$

where

$$\Delta q = \frac{2\pi}{L}. \tag{C5}$$

Then,

$$A_\rho(q_1) = \frac{2\pi}{\rho_0}B_\rho(q_1), \tag{C6}$$

Thus,

$$g(r) - 1 = \frac{1}{2\pi^2\rho_0 r}\int [S(Q) - 1]Q \sin(Qr)dQ$$
$$= \frac{A_\rho(q_1)}{2\pi^2\rho_0 r}q_1 \sin(q_1 r) = B_\rho(q_1)\frac{{q_1}^2}{\pi{\rho_0}^2}\frac{\sin(q_1 r)}{q_1 r}. \quad \text{(C7)}$$

REFERENCES

[1] P. A. Egelstaff, *An Introduction to the Liquid State*, 1st ed.; 2nd ed. (Academic Press; Oxford University Press, Oxford, 1967; 1991).
[2] C. A. Croxton, *Liquid State Physics: A Statistical Mechanical Introduction* (Cambridge University Press, Cambridge, 1974).
[3] J.-P. Hansen and I. R. McDonald, *Theory of Simple Liquids* (Academic Press, London, 1976; 1986; 2006).
[4] P. G. Debenedetti and F. H. Stillinger, Nature **410**, 259 (2001).
[5] G. Parisi, P. Urbani, and F. Zamponi, *Theory of Simple Glasses: Exact Solutions in Infinite Dimensions* (Cambridge University Press, Cambridge, 2020).
[6] B. E. Warren, *X-Ray Diffraction* (Addison-Wesley, Reading, 1969).
[7] S. C. Glotzer, V. N. Novikov, and T. B. Schröder, J. Chem. Phys. **112**, 509 (2000).
[8] J.-P. Bouchaud and G. Biroli, J. Chem. Phys. **121**, 7347 (2004).
[9] S. Albert, T. Bauer, M. Michl, G. Biroli, J.-P. Bouchaud, A. Loidl, P. Lunkenheimer, R. Tourbot, C. Wiertel-Gasquet, and F. Ladieu, Science **352**, 1308 (2016).
[10] J. D. Bernal and J. Mason, Nature **188**, 910 (1960).
[11] D. R. Nelson, Phys. Rev. B **28**, 5515 (1983).
[12] D. B. Miracle, Nat. Mater. **3**, 697 (2004).
[13] H. W. Sheng, W. K. Luo, F. M. Alamgir, J. M. Bai, and E. Ma, Nature **439**, 419 (2006).
[14] S. Im, Y. Wang, P. Zhao, G. H. Yoo, Z. Chen, G. Calderon, M. Abbasi Gharacheh, M. Zhu, O. Licata, B. Mazumder, D. A. Muller, E. S. Park, Y. Wang, and J. Hwang, Phys. Rev. Mater. **5**, 115604 (2021).
[15] J. M. Gibson, M. M. J. Treacy, and P. M. Voyles, Ultramicroscopy **83**, 169 (2000).
[16] J. Ding, E. Ma, M. Asta, and R. O. Ritchie, Sci. Rep. **5**, 17429 (2015).
[17] H. Lou, X. Wang, Q. Cao, D. Zhang, J. Zhang, T. Hu, H.-k. Mao, and J.-Z. Jiang, Proc. Natl. Acad. Sci. U. S. A. **110**, 10068 (2013).
[18] S. Wei, M. Stolpe, O. Gross, Z. Evenson, I. Gallino, W. Hembree, J. Bednarcik, J. J. Kruzic, and R. Busch, Appl. Phys. Lett. **106**, 181901 (2015).
[19] T. Egami and C. W. Ryu, Phys. Rev. E **104**, 064109 (2021).
[20] G. S. Cargill III, Solid State Phys. **30**, 227 (1975).
[21] T. Egami, Front. Phys. **8**, 50 (2020).
[22] B. Wu, T. Iwashita, and T. Egami, Phys. Rev. Lett. **120**, 135502 (2018).
[23] L. Van Hove, Phys. Rev. **95**, 249 (1954).
[24] S. Alexander and J. McTague, Phys. Rev. Lett. **41**, 702 (1978).
[25] S. Sachdev and D. R. Nelson, Phys. Rev. B **32**, 4592 (1985).
[26] T. Egami and C. W. Ryu, Front. Mater. **9**, 874191 (2022).
[27] T. Egami and C. W. Ryu, J. Phys.: Condens. Matter **35**, 174002 (2023).
[28] P. S. Salmon, A. C. Barnes, R. A. Martin, and G. J. Cuello, Phys. Rev. Lett. **96**, 235502 (2006).
[29] D. Ma, A. D. Stoica, and X.-L. Wang, Nat. Mater. **8**, 30 (2009).
[30] P. Chirawatkul, A. Zeidler, P. S. Salmon, S. Takeda, Y. Kawakita, T. Usuki, and H. E. Fischer, Phys. Rev. B **83**, 014203 (2011).
[31] S. V. Sukhomlinov and M. H. Müser, Phys. Rev. Mater. **2**, 115604 (2018).
[32] C. W. Ryu, W. Dmowski, K. F. Kelton, G. W. Lee, E. S. Park, J. R. Morris, and T. Egami, Sci. Rep. **9**, 18579 (2019).
[33] C. W. Ryu and T. Egami, Phys. Rev. E **102**, 042615 (2020).
[34] C. A. Angell, Science **267**, 1924 (1995).
[35] T. Egami and C. W. Ryu, Front. Chem. **8**, 579169 (2020).
[36] T. Egami and C. W. Ryu, Phys. Rev. E **104**, 064110 (2021).
[37] W. Götze, *Complex Dynamics of Glass-Forming Liquids* (Oxford University Press, Oxford, 2009).
[38] E. Leutheusser, Phys. Rev. A **29**, 2765 (1984).
[39] S. P. Das, Rev. Mod. Phys. **76**, 785 (2004).
[40] A. J. Liu and S. R. Nagel, Nature **396**, 21 (1998).
[41] G. Parisi and F. Zamponi, Rev. Mod. Phys. **82**, 789 (2010).
[42] T. R. Kirkpatrick and P. G. Wolynes, Phys. Rev. A **35**, 3072 (1987).
[43] X. Xia and P. G. Wolynes, Phys. Rev. Lett. **86**, 5526 (2001).
[44] V. Lubchenko and P. G. Wolynes, Annu. Rev. Phys. Chem. **58**, 235 (2007).
[45] P. G. Wolynes and V. Lubchenko, *Structural Glasses and Supercooled Liquids* (John Wiley and Sons 2012).
[46] L. S. Ornstein and F. Zernike, Proc. R. Neth. Acad. Arts Sci. **17**, 793 (1914).
[47] J. K. Percus and G. J. Yevick, Phys. Rev. **110**, 1 (1958).
[48] J. S. Rowlinson, Rep. Prog. Phys. **28**, 169 (1965).
[49] S. Chakrabarty and Z. Nussinov, Phys. Rev. B **84**, 064124 (2011).
[50] C. W. Ryu, W. Dmowski, and T. Egami, Phys. Rev. E **101**, 030601(R) (2020).
[51] P. Kleban, J. Stat. Phys. **11**, 317 (1974).
[52] R. L. McGreevy, J. Phys.: Condens. Matter **13**, R877 (2001).
[53] P. M. Chaikin and T. C. Lubensky, *Principles of Condensed Matter Physics* (Cambridge University Press, Cambridge, 1995).
[54] D. Srolovitz, K. Maeda, V. Vitek, and T. Egami, Philos. Mag. A **44**, 847 (1981).
[55] M. Goldstein, J. Chem. Phys. **51**, 3728 (1969).
[56] D. Shechtman, I. Blech, D. Gratias, and J. W. Cahn, Phys. Rev. Lett. **53**, 1951 (1984).
[57] D. Levine and P. J. Steinhardt, Phys. Rev. Lett. **53**, 2477 (1984).
[58] T. Aste and D. Sherrington, J. Phys. A: Math. Gen. **32**, 7049 (1999).
[59] M. I. Ojovan and W. E. Lee, J. Phys.: Condens. Matter **18**, 11507 (2006).
[60] T. Iwashita, D. M. Nicholson, and T. Egami, Phys. Rev. Lett. **110**, 205504 (2013).
[61] T. Egami, Mod. Phys. Lett. B **28**, 1430006 (2014).
[62] J. D. Eshelby, Proc. R. Soc. London, Ser. A **241**, 376 (1957).
[63] T. Egami, K. Maeda, and V. Vitek, Philos. Mag. A **41**, 883 (1980).
[64] S.-P. Chen, T. Egami, and V. Vitek, Phys. Rev. B **37**, 2440 (1988).
[65] V. A. Levashov, T. Egami, R. S. Aga, and J. R. Morris, Phys. Rev. B **78**, 064205 (2008).
[66] T. Egami and Y. Waseda, J. Non-Cryst. Solids **64**, 113 (1984).
[67] T. Egami and S. Aur, J. Non-Cryst. Solids **89**, 60 (1987).
[68] K. Maeda and S. Takeuchi, J. Phys. F: Met. Phys. **8**, L283 (1978).
[69] J. Ding, M. A. Asta, and R. O. Ritchie, Proc. Natl. Acad. Sci. U. S. A. **114**, 8458 (2017).
[70] D. Kivelson, S. A. Kivelson, X. Zhao, Z. Nussinov, and G. Tarjus, Physica A **219**, 27 (1995).
[71] E. Donth, *The Glass Transition: Relaxation Dynamics of Liquids and Disordered Materials* (Springer, Berlin, 2010).
[72] G. Adam and J. H. Gibbs, J. Chem. Phys. **43**, 139 (1965).
[73] A. Montanari and G. Semerjian, J. Stat. Phys. **125**, 23 (2006).
[74] A. S. Argon, Acta Metall. **27**, 47 (1979).
[75] M. L. Falk and J. S. Langer, Phys. Rev. E **57**, 7192 (1998).
[76] A. Widmer-Cooper and P. Harrowell, Phys. Rev. Lett. **96**, 185701 (2006).
[77] M. H. Cohen and D. Turnbull, J. Chem. Phys. **31**, 1164 (1959).
[78] E. D. Cubuk, S. S. Schoenholz, J. M. Rieser, B. D. Malone, J. Rottler, D. J. Durian, E. Kaxiras, and A. J. Liu, Phys. Rev. Lett. **114**, 108001 (2015).
[79] V. Bapst, T. Keck, A. Grabska-Barwińska, C. Donner, E. D. Cubuk, S. S. Schoenholz, A. Obika, A. W. R. Nelson, T. Back, D. Hassabis, and P. Kohli, Nat. Phys. **16**, 448 (2020).
[80] M. L. Manning and A. J. Liu, Phys. Rev. Lett. **107**, 108302 (2011).
[81] C. Liu and Y. Fan, Phys. Rev. Lett. **127**, 215502 (2021).
[82] J. Ding, L. Li, N. Wang, L. Tian, M. Asta, R. O. Ritchie, and T. Egami, Mater. Today Phys. **17**, 100359 (2021).
[83] Y. Fan, T. Iwashita, and T. Egami, Nat. Commun. **8**, 15417 (2017).
[84] J. F. Mason and P. T. Piiroinen, Chaos **22**, 013106 (2012).
[85] H. Párraga, F. J. Arranz, R. M. Benito, and F. Borondo, J. Phys. Chem. A **122**, 3433 (2018).
[86] P. Charbonneau, J. Kurchan, G. Parisi, P. Urbani, and F. Zamponi, Nat. Commun. **5**, 3725 (2014).

[87]P. Cao, M. P. Short, and S. Yip, Proc. Natl. Acad. Sci. U. S. A. **116**, 18790 (2019).
[88]Y. Suzuki and T. Egami, J. Non-Cryst. Solids **75**, 361 (1985).
[89]T. Egami, T. Iwashita, and W. Dmowski, Metals **3**, 77 (2013).
[90]S. Torquato, Phys. Rep. **745**, 1 (2018).
[91]S. Torquato and F. H. Stillinger, Phys. Rev. E **68**, 041113 (2003).
[92]A. B. Hopkins, F. H. Stillinger, and S. Torquato, Phys. Rev. E **86**, 021505 (2012).
[93]E. Marcotte, F. H. Stillinger, and S. Torquato, J. Chem. Phys. **138**, 12A508 (2013).
[94]E. Tjhung and L. Berthier, Phys. Rev. Lett. **114**, 148301 (2015).
[95]G. Zhang, F. H. Stillinger, and S. Torquato, Sci. Rep. **6**, 36963 (2016).
[96]G. Zhang, F. H. Stillinger, and S. Torquato, Phys. Rev. E **96**, 042146 (2017).
[97]D. Hexner, P. M. Chaikin, and D. Levine, Proc. Natl. Acad. Sci. U. S. A. **114**, 4294 (2017).
[98]S. Mitra, A. D. S. Parmar, P. Leishangthem, S. Sastry, and G. Foffi, J. Stat. Mech.: Theory Exp. **2021**, 033203.